

RESEARCH ARTICLE

Learning to define an electrical biomarker of the epileptogenic zone

Jian Li¹  | Olesya Grinenko²  | John C. Mosher³  | Jorge Gonzalez-Martinez²  | Richard M. Leahy¹  | Patrick Chauvel² 

¹Signal and Image Processing Institute, University of Southern California, Los Angeles, California

²Epilepsy Center, Cleveland Clinic Neurological Institute, Cleveland, Ohio

³Department of Neurology, University of Texas Health Science Center at Houston, Houston, Texas

Correspondence

Patrick Chauvel, Epilepsy Center, Cleveland Clinic Neurological Institute, 9500 Euclid Avenue, Cleveland, OH 44195.
Email: chauvel@ccf.org

Funding information

National Institutes of Health, Grant/Award Numbers: R01-EB026299, R01-EB009048, R01-NS089212

Abstract

The role of fast activity as a potential biomarker in localization of the epileptogenic zone (EZ) remains controversial due to recently reported unsatisfactory performance. We recently identified a “fingerprint” of the EZ as a time-frequency pattern that is defined by a combination of preictal spike(s), fast oscillatory activity, and concurrent suppression of lower frequencies. Here we examine the generalizability of the fingerprint in application to an independent series of patients (11 seizure-free and 13 non-seizure-free after surgery) and show that the fingerprint can also be identified in seizures with lower frequency (such as beta) oscillatory activity. In the seizure-free group, only 5 of 47 identified EZ contacts were outside the resection. In contrast, in the non-seizure-free group, 104 of 142 identified EZ contacts were outside the resection. We integrated the fingerprint prediction with the subject's MR images, thus providing individualized anatomical estimates of the EZ. We show that these fingerprint-based estimates in seizure-free patients are almost always inside the resection. On the other hand, for a large fraction of the nonseizure-free patients the estimated EZ was not well localized and was partially or completely outside the resection, which may explain surgical failure in such cases. We also show that when mapping fast activity alone onto MR images, the EZ was often over-estimated, indicating a reduced discriminative ability for fast activity relative to the full fingerprint for localization of the EZ.

KEYWORDS

epileptogenic zone, high-frequency oscillations, localization-related epilepsy, partial seizure, stereo-EEG

1 | INTRODUCTION

New vistas in the pathophysiology of focal epilepsies and attempts to improve the localization of the epileptogenic zone (EZ) in epilepsy surgery converge on a common question: What is the role of high-frequency cortical activity in seizure initiation? After the identification

of interictal fast ripples as a potential marker for epileptogenicity, several clinical studies have investigated their possible colocalization with the seizure onset using statistical approaches. However, a consistently identifiable transition from interictal high-frequency activity (HFA) and/or spikes to seizure development is far from evident in practice (González Otárola, von Ellenrieder, Cuello-Oderiz, Dubeau, & Gotman,

This is an open access article under the terms of the Creative Commons Attribution-NonCommercial License, which permits use, distribution and reproduction in any medium, provided the original work is properly cited and is not used for commercial purposes.

© 2019 The Authors. *Human Brain Mapping* published by Wiley Periodicals, Inc.

2019). Therefore, a clearer definition of the “seizure onset” is of high importance as it is both a prerequisite to validate interictal features and a rational basis to delineate the EZ. Even though various modes of onset can be observed (Lagarde et al., 2019; Singh, Sandy, & Wiebe, 2015), a feature generally acknowledged by all authors is the sharp or progressive frequency pattern change to a higher frequency range in some areas, often called the “seizure onset zone” (SOZ).

Defining a bio-electrical marker for the EZ is both useful for epilepsy surgery and meaningful for understanding the pathophysiology of epilepsy. An accurate marker would help to fill the gap between “intracranial EEG” phenomenological classifications and neurophysiological or modeling studies.

Several attempts to measure the EZ extent based on “stereotactically implanted EEG” (SEEG) signal processing have been made over the past decade. Bartolomei, Chauvel, and Wendling (2008) proposed to quantify the relative onset times of the fast activity (FA) recorded in different areas. Detecting spectral changes during the preictal to ictal transition, the signal energy ratio between high and low-frequency bands was calculated and its detection time plotted in each recording channel. Application to mesial temporal lobe epilepsies as opposed to “lateral” temporal lobe epilepsies differentiated epileptogenicity among the two localizations. David et al. (2011) undertook a neuroimaging study to represent an epileptogenicity index based on quantification of the HFA using statistical parametric mapping. This study allowed mapping of the location of the fastest activities and their “slow propagation” during peri-onset time, and comparison with the surgically resected area. This work added to the validation of HFA as a marker of SOZ. A different approach of “frequency localization” was used by Gnatkovsky et al. (2011), considering that frequency changes in different bands may occur successively or simultaneously during seizure onset. Therefore, the EZ, defined as the area of frequency changes at seizure onset, could be delineated whatever the peculiarity of frequency patterns recorded in different seizures in a given patient. In a prospective study of patients investigated with SEEG (Gnatkovsky et al., 2014), the same method was applied to test three biomarkers of the EZ, namely HFA, signal flattening, and slow potential shift. These biomarkers colocalized with the location of the EZ as defined by standard neurophysiological means and postsurgical seizure outcome. However, the three markers were analyzed as discrete phenomena, even though the HFA and the slow potential shift are probably related, the signal flattening proved not to be discriminative.

We recently identified a “fingerprint” of the EZ via a time-frequency (TF) approach in a series of patients who were evaluated with SEEG and were seizure-free (SF) after surgery (Grinenko et al., 2018). A TF pattern of the interictal to ictal transition was common across all patients inside the resected areas. Although this pattern included narrow-band FA, the discriminating factor was the combination of FA with preictal spike(s) and simultaneous suppression of lower frequencies (see Supporting Information for a summary of the feature definition and extraction procedure). Based on the EZ fingerprint pattern, a support vector machine (SVM)-based classification

algorithm was developed to automatically identify features of the fingerprint pattern and distinguish EZ from non-EZ contacts.

Since the EZ fingerprint was demonstrated in SF patients with ictal FA in the gamma band, some questions still remain unanswered: is the EZ fingerprint a common feature of all focal seizures, even for seizure onset patterns with oscillatory activity in a lower frequency range? Would the EZ fingerprint be recorded outside the resected region in nonseizure-free (NSF) patients, meaning that surgical failures can be explained by the fact that fingerprint-positive areas were not resected? Previous studies had treated FA as a single category, whereas Grinenko et al. (2018) showed a distinction between broad-band and narrow-band gamma activity. Hence, a comparison between the accuracy of narrow-band FA identified by our method and the EZ fingerprint in localizing the EZ is needed.

In this study we evaluate the performance of the original EZ fingerprint method on a new broader population of patients, including both SF and NSF patients. We show that the EZ fingerprint can be identified in patients with oscillatory activities as low as beta or alpha frequency. Classification results show substantial difference between the SF and NSF groups, with the latter group revealing a large number of EZ contacts predicted outside the resection region. We also extend the EZ fingerprint method to an end-to-end classification pipeline by interpolating the prediction scores onto individual patient's MR images, which allows us to predict and visualize the extent of the EZ with respect to individual anatomy. By applying this extended EZ fingerprint pipeline, we demonstrate that fingerprint-based EZ anatomical estimates present as well-circumscribed areas globally located inside the resected region in SF patients. In contrast for NSF patients, the estimated EZ is not well localized and is located partially or completely outside the resection, which may explain the surgical failure. Furthermore, when using only FA, but otherwise following the same extended EZ fingerprint pipeline, we show that the extent of the EZ can be over-estimated.

2 | METHODS

2.1 | Patient selection and data collection

Working under a protocol approved by the Institutional Review Board, we included a consecutive series of 24 patients in year 2015 who had seizures that began with low voltage FA in the beta or gamma bands and were operated on after SEEG evaluation. The details of the patient selection protocol are presented in Figure S1.

SEEG is an invasive presurgical procedure for patients with pharmaco-resistant focal epilepsy. Anatomico-electro-clinical hypotheses were formulated individually for each patient during a multidisciplinary patient management conference based on available noninvasive data: clinical history, video EEG, MRI, PET, ictal SPECT, and MEG. Multilead depth electrodes (AdTech, Racine, WI; Integra, Plainsboro, NJ; or PMT, Chanhassen, MN) were implanted according to the Talairach stereotactic method. SEEG signals were recorded on a Nihon Kohden (Irvine, CA) EEG machine with a sampling rate of 1,000 Hz.

Anatomical locations of the electrode leads were identified by a digital fusion of the postimplantation thin-sliced CT image with the preoperative T1-weighted MR image using CURRY 7 (Compumedics NeuroScan, Hamburg, Germany) and visualized on the preoperative MR image using Brainstorm (Tadel, Baillet, Mosher, Pantazis, & Leahy, 2011). A postoperative MR image was also acquired after the surgery (except for Subject 231 where a postoperative CT image was acquired) and rigidly coregistered to the postimplantation CT image to identify the positions of the electrode contacts with respect to the location of the resected/ablated region.

2.2 | EZ fingerprint pipeline for individualized EZ prediction

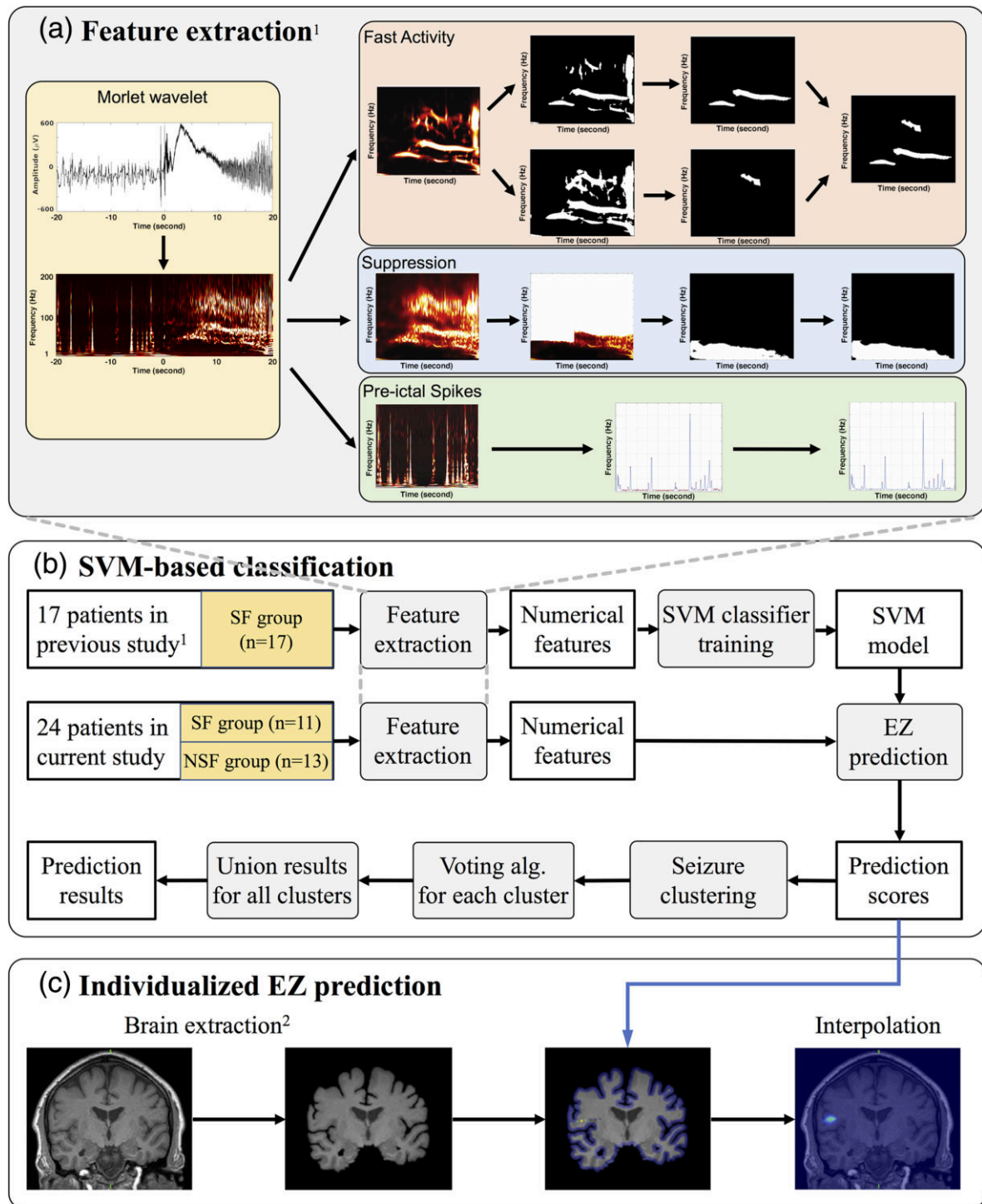
In our previous study (Grinenko et al., 2018), we described an EZ fingerprint method that distinguished electrode contacts within the EZ from non-EZ contacts (open-source software was developed and released for research purpose only, available at: https://silencer1127.github.io/software/EZ_Fingerprint/ezf_main). The fingerprint method has also been integrated into the Brainstorm software: <https://neuroimage.usc.edu/brainstorm/>). We approached the problem by first transforming the raw ictal SEEG time series into TF representations using the Morlet wavelet transform, followed by an artifact removal procedure using complex independent component analysis. We also selected a segment of spontaneous baseline data at least 2 min before the seizure, where no obvious seizure or spiking activity or artifacts were identified and transformed this baseline segment into TF maps as well. We then normalized the seizure TF maps against the baseline maps for each frequency. The normalized TF maps were then used to extract three distinct features: FA, suppression, and preictal spikes, illustrated in Figure 1. Finally, an SVM classifier was trained on a combination of the three features and a leave-one-subject-out cross-validation was performed on a set of 17 patients who had seizures with sustained gamma activity and were SF after surgery. The analysis pipeline is described in full in Grinenko et al. (2018) and an abridged summary of the feature extraction methodology is included here in the Supporting Information.

Here we use an extension of the EZ fingerprint method, illustrated in Figure 1, that incorporates anatomical information into the prediction by mapping the prediction scores onto the patient's MR image, hence offering a complete end-to-end classification pipeline that starts with preprocessing of the raw SEEG signals and yields an individualized prediction and visualization of the EZ overlaid on the patient's MR image. The prediction scores from the trained SVM model in the previous EZ fingerprint pipeline offer a continuous predicted value (a scalar-valued measure) for each contact, roughly reflecting how likely that contact is to be in the EZ. A positive score indicates a higher probability, a negative score indicates a lower probability, and a zero score shows maximal uncertainty about whether the contact is in the EZ or not. The extension starts with coregistration of the postimplantation CT image to the patient's preoperative MR image so that the electrode contacts are aligned to the MRI space. Then, we extract a masked brain (cerebrum and cerebellum

only) from the MR image using the skull stripping tool provided in BrainSuite (Shattuck & Leahy, 2002). To perform the interpolation, we first set the value of the brain's boundary voxels to the minimal predicted scores across all contacts and the value of the nearest voxel to each contact location to be the corresponding predicted score for that contact. We then interpolate the values for all other voxels inside the brain mask using linear interpolation between the contact locations and brain boundary values. Interpolation was computed using Delaunay triangulation (Amidror, 2002) as provided by the "scatteredInterpolant" function in MATLAB (the Mathworks, Inc., Natick, MA). See Figure 1c.

In this study we evaluate effectiveness of the EZ fingerprint on a completely independent consecutive series of patients that underwent SEEG evaluation in 2015, including both SF and NSF groups. First, the SVM-based model was trained using the patient data from our previous study (Grinenko et al., 2018). We then processed all available seizures for the 24 patients in the current study using the pipeline in Figure 1 to compute the SVM-based EZ scores. These scores were then thresholded to identify EZ contacts. We also manually labeled contacts as being within or outside the resected area based on the patient's coregistered postoperative MR image. Finally, we compared the predicted labels with the resection labels.

Intrasubject variation of time-series characteristics of ictal patterns, as exemplified in Figure 2a, can significantly affect prediction results and lead to underestimation of the EZ. Such a variation does not affect SEEG visual analysis as the expert classifies them as the same seizure type but with subtle waveform alterations or different latencies in the propagation network. However, the SVM classifier is sensitive to such formal variation. To take this variation into consideration, a clustering of seizures was performed for each subject as follows: for each seizure, we first applied the EZ fingerprint pipeline to the ictal time series (Figure 2a) to obtain a prediction score (Figure 2b) for each contact from the trained SVM model. We computed the cross-correlations of the prediction scores for each subject across the electrode array between all pairs of seizures. Figure 2c shows an example of the cross-correlation matrix among all five seizures for Subject 112. By visual inspection, the five seizures naturally fall into two clusters: Seizures 1 and 3 and Seizures 2, 4, and 5 (Figure 2d). These two groups show high intracluster correlation while the correlation between the two clusters is weak. For most patients the number of clusters and their membership is clear by inspection of the correlation matrix. An automated method based on *k*-means clustering could be used for this purpose, but we found that user-based clustering was sufficient. We note that since this was done without reference to the resected region or surgical outcomes, there is no concern that we may be biasing our results by using manual clustering. The clustering procedure was performed for all 24 subjects. We then evaluated prediction performance by identifying the EZ contacts using the EZ fingerprint separately for each cluster and then taking the union of the prediction results, that is, a contact is finally predicted to be in the EZ area if it is identified as an EZ contact in any of the clusters of seizures, Figure 1b.



¹ Grinenko O, *et al.* "A fingerprint of the epileptogenic zone in human epilepsies." *Brain* 2018; 141: 117-131.

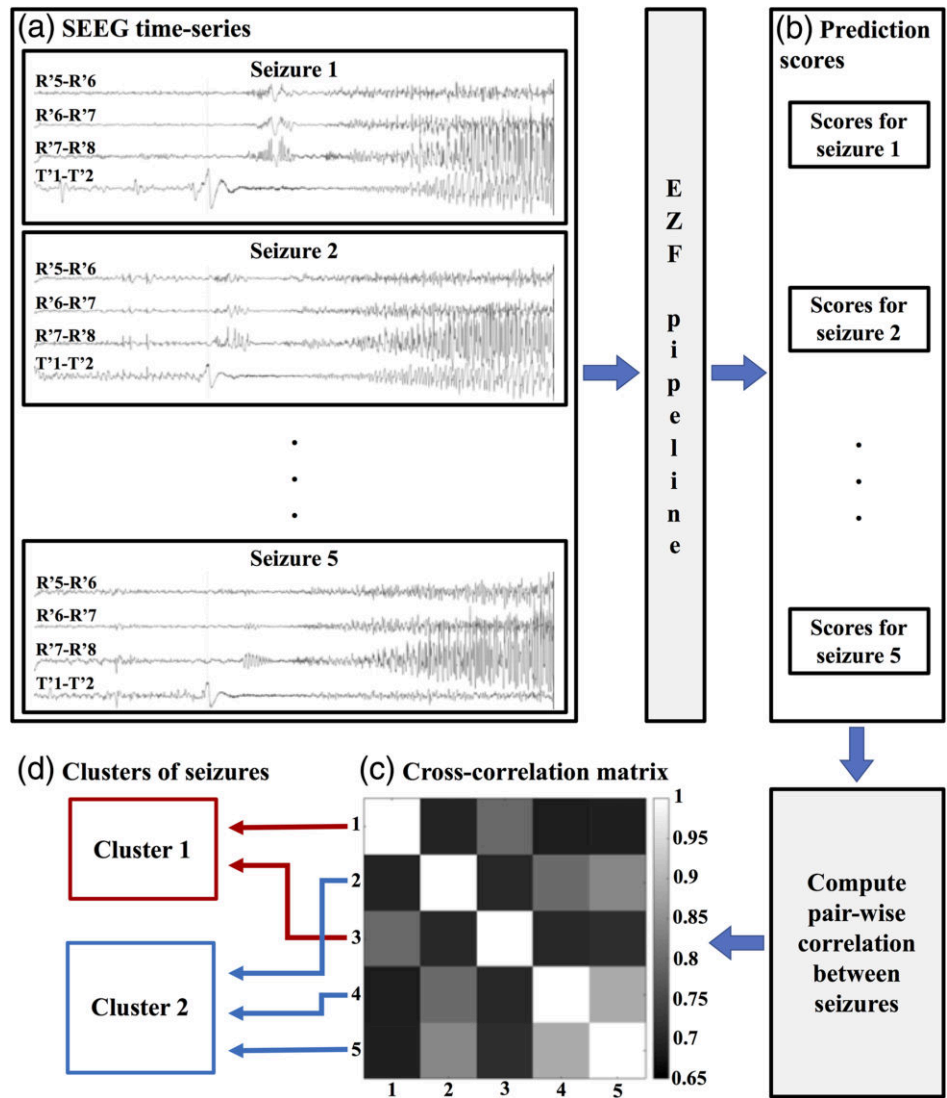
² Shattuck DW, Leahy RM. "BrainSuite: An automated cortical surface identification tool." *Med. Image Anal.* 2002; 6: 129-142.

FIGURE 1 Epileptogenic zone fingerprint pipeline. (a) Feature extraction for fast activity, suppression and preictal spikes from time-frequency maps; (b) Classification procedures where an SVM model was trained using the original 17 subjects in the previous study and the EZ was predicted for the 24 new subjects in the current study; (c) Interpolation of prediction scores onto patient's individual MR images. EZ, epileptogenic zone; SVM, support vector machine [Color figure can be viewed at wileyonlinelibrary.com]

To address the question of whether FA alone can differentiate EZ contacts from non-EZ contacts, as is commonly practiced in SEEG, we compared the performance of the pipeline using the fingerprint versus

FA alone (top-right "FAs" subblock in Figure 1a) as the feature in the SVM-based classification. Note that the features we used for FA are based on our own characterization of the narrow-band FA as

FIGURE 2 An example of the seizure clustering procedure for Subject 112. (a) Ictal time series illustrating variations in ictal patterns: Isolated preictal spiking only in channel T' in Seizure 1 and continuous preictal spiking synchronous between channel T' and R' in Seizures 2 and 5; (b) Prediction scores obtained individually for each seizure; (c) Cross-correlations of the prediction scores across the electrode array between all pairs of seizures (five seizures in total for this subject); (d) Manual clustering of seizures according to cross-correlation matrix [Color figure can be viewed at wileyonlinelibrary.com]



described in Grinenko et al. (2018) rather than the energy of the entire gamma band. In total there are 17 numerical descriptors extracted for FA, including number of narrow bands, the maximum/minimum frequency, the starting/ending time, and the orientation of the FA bands (see the supplementary materials in Grinenko et al. (2018) for complete details). We also linearly mapped the maximum frequency (one of the 17 numerical descriptors in feature extraction step) of the FA onto the patient's MRI space for visualization and comparison purposes.

To statistically test the difference of the predicted EZ (in the MRI space) between the SF and NSF group, we calculated the kurtosis of the distribution of interpolated predicted EZ scores over the entire masked brain for each subject. "Kurtosis" is a measure of the "tailedness" of probability distributions (Westfall, 2014) and sensitive to outliers. The higher the kurtosis, the more localized the predicted EZ is and the higher prediction score within the predicted EZ area.

We also compared the anatomical prediction results with surgical outcomes (Engel score). For each patient, we first predicted the EZ using the extended EZ fingerprint pipeline. Then we manually

examined the relationship between the predicted EZ area and the resected area (hereafter the "relationship"), determining either that the predicted EZ was fully resected, partially resected, or not resected.

3 | RESULTS

In total, 24 subjects met the patient selection criteria (Figure S1), 11 of them became SF, and the remaining 13 had seizure recurrence after surgery, that is, NSF. Table 1 shows the clinical profiles of the subjects included in this study. We analyzed all available seizures, except in cases where patients had more than 10 consecutive seizures, then only the first 10 seizures were analyzed. Nine subjects had additional seizures without initial FA that were not included in the study (additional information for these seizures is shown in Table S1).

All 24 subjects had seizure onset from low voltage FA. Figure 3 shows the statistics of the maximum and minimum frequency of FA. The median of the maximum frequency of FA was 74 Hz with an interquartile range (IQR) 25 Hz, and the median of the minimum

TABLE 1 Clinical profiles of the patients

Subject ID ^a	Age (years)	Epilepsy duration (years)	MRI lesion	Surgical pathology	Resection (or ablation) details	Outcome	Follow-up duration (months)
101	25	11	Normal	Focal gliosis	L lateral temporal cortexectomy	Seizure-free	27
102	17	7	Normal	FCD Type 1	L temporal polar and amygdala resection	Seizure-free	36
103	30	12	Normal	FCD Type 1	R anterior temporal lobectomy	Seizure-free	36
106	17	9	Normal	FCD Type 2B	R SMA/cingulate resection	Seizure-free	28
108	37	32	Suspected FCD	FCD Type 2B	R subcentral resection	Seizure-free	20
111	48	6	Normal	FCD Type 1	L anterior temporal lobectomy	Seizure-free	28
112	21	18	Normal	No due to laser surgery	L insular/temporal/frontal operculum laser ablation	Seizure-free	31
113	24	17	Suspected FCD	FCD Type 1	R anterior temporal lobectomy	Seizure-free	29
116	11	7	Prior resection, otherwise normal	Gliosis	R insular/ fronto-parietal and temporal operculum	Seizure-free	22
118	33	13	Normal	Gliosis	R prefrontal resection	Seizure-free	19
140	39	3	Normal	Focal perivascular gliosis	Anterior temporal lobectomy	Seizure-free	21
215 ^b	35	4	PNH	No due to laser surgery	Laser ablation, periventricular nodule	Seizures	
219 ^c	30	5	Normal	No due to laser surgery	Laser ablation, L cingulate/SMA	One-year seizure-free then seizure recurred	
220	38	22	Normal	FCD Type 1	R posterior basal temporal resection	Seizures	
221	41	39	Normal	Gliosis	R lateral temporo-parietal resection	Seizures	
222	24	14	Normal	FCD Type 1	R basal posterior temporal resection	One-year seizure-free then seizure recurred	
223	6	2	Normal	Inflammation, FCD Type 1	L anterior lateral temporal resection	Seizures	
226	24	18	Normal	FCD Type 1	L prefrontal resection	Seizures	
228 ^b	25	12	Multiple areas of gliosis	Gliosis	R parieto-occipital resection	Seizures	
231 ^c	34	34	Normal	No due to laser surgery	Laser ablation, L frontal operculum	Seizures	
232 ^b	10	10	Bilateral occipital lesion	Ulegyria, inflammation	L parieto-occipital resection	Seizures	
233	29	10	Heterotopic gray matter	FCD Type 1	R temporooccipital resection	Seizures	
237	20	16	Normal	No due to laser surgery	Laser ablation, R angular gyrus	Seizures	
238	35	35	PMG	No due to laser surgery	Laser ablation, L fronto-parietal operculum, subcentral gyrus	Seizures	

Abbreviations: FCD, focal cortical dysplasia; L, left; PMG, polymicrogyria; PNH, periventricular nodular heterotopia; R, right; SMA, supplemental motor area.

^aSubjects from 101 to 140 were seizure-free (SF) after the surgery and subjects from 215 to 238 were nonseizure-free (NSF).

^bPatients had seizures initiated from different area than fast activity, which influenced the surgery planning.

^cSparse implantation with inadequate sampling of the epileptogenic zone.

frequency of FA was 45 Hz with an IQR 22 Hz. Of the 11 SF patients, the full fingerprint pattern was observed from the TF plots in 9 patients and partially observed, that is, only one or two out of the three components (FA, suppression, preictal spikes) in the other 2 patients. Of the 13 NSF patients, the full fingerprint pattern was

observed in 10 patients, partially observed in 1 patient, and missed in the other 2 patients.

Table 2a shows classification results using the EZ fingerprint method for all 24 subjects. These results are based on analysis in which seizures are clustered for each subject to determine the EZ as

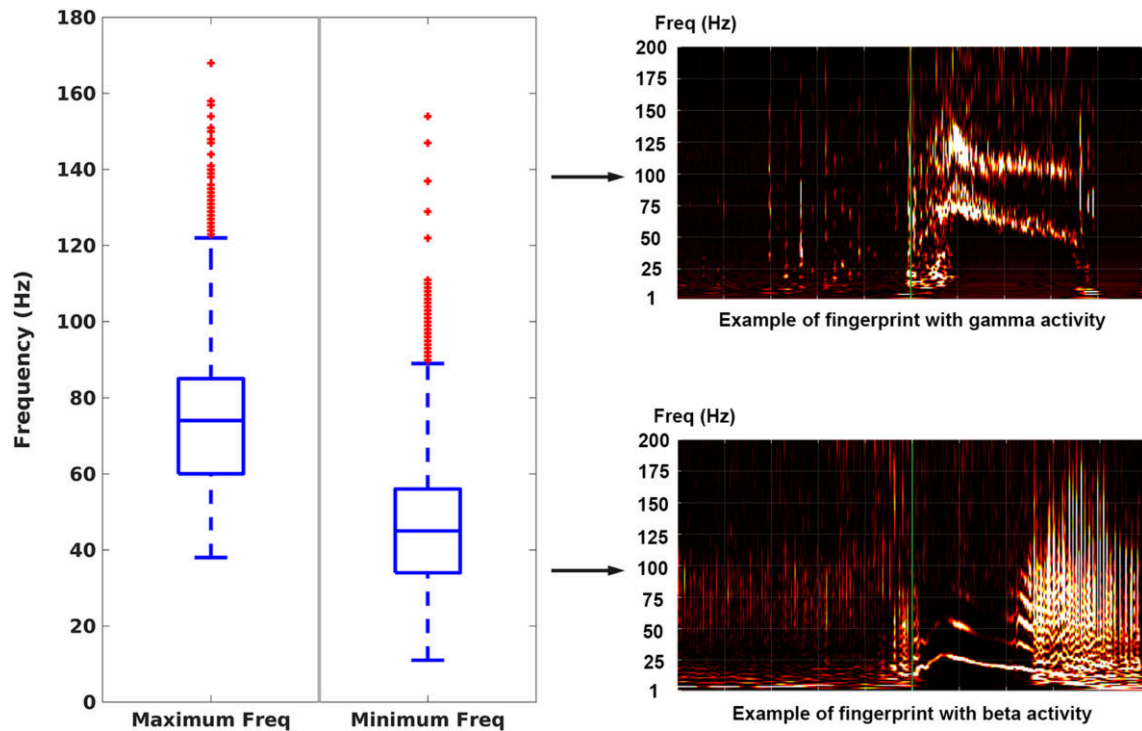


FIGURE 3 Statistics of the maximum frequency and minimum frequency of fast activity. Examples of identified fingerprint pattern with gamma activity and beta activity are shown on the right [Color figure can be viewed at wileyonlinelibrary.com]

TABLE 2 Epileptogenic zone fingerprint prediction results and comparison with that using fast activity only

(a) Prediction results using epileptogenic zone fingerprint						
	Seizure-free patients			Nonseizure-free patients		
	Prediction true	Prediction false	Statistics	Prediction true	Prediction false	Statistics
Inside resection	42 (TP ^a)	267 (FN ^a)		38 (TP ^a)	104 (FN ^a)	
Outside resection	5 (FP ^a)	838 (TN ^a)	0.006 (FPR)	104 (FP ^a)	1,276 (TN ^a)	0.075 (FPR)
Statistics	0.894 (PPV)			0.268 (PPV)		
(b) Prediction results using features from fast activity only						
	Seizure-free patients			Nonseizure-free patients		
	Prediction true	Prediction false	Statistics	Prediction true	Prediction false	Statistics
Inside resection	181 (TP ^a)	128 (FN ^a)		147 (TP ^a)	94 (FN ^a)	
Outside resection	281 (FP ^a)	562 (TN ^a)	0.333 (FPR)	693 (FP ^a)	687 (TN ^a)	0.502 (FPR)
Statistics	0.392 (PPV)			0.175 (PPV)		

Abbreviations: FN, false negative; FP, false positive; FPR, false positive rate; PPV, positive predictive value; TN, true negative; TP, true positive.

^aTP/FP/TN/FN are with respect to the resected region rather than the actual EZ.

described above. For the SF group, we were able to achieve a similar performance to that in our original report (Grinenko et al., 2018). Our EZ fingerprint identified the EZ in 8 of 11 SF patients. In total, only five electrode contacts from two subjects (Subject 102 and 113) were identified as EZ contacts outside the resected area (in the other six subjects, the EZ was predicted strictly inside the resection), yielding 89.4% positive predictive value (PPV) and 0.6% false positive rate (FPR). For the three remaining subjects no EZ contact was predicted. The EZ fingerprint is apparently present

for at least one subject (Subject 103 in Figure S2) but was not classified as such by the SVM. This missed detection is because the feature detection and classification pipeline was trained on the data from (Grinenko et al., 2018) which used more restrictive inclusion criteria that may have led to failure to detect this fingerprint. The fingerprint was, at best, only partially observed in the other two subjects (Subject 101 and 140 in Figure S2). We hypothesize that we did not have electrode contacts inside (or close to) the EZ area. However, a large surgical resection was

performed, and the two patients were SF after the surgery, indicating that EZ was removed, even though not directly sampled by the SEEG electrodes.

In contrast, for the NSF group, 104 out of 142 electrode contacts were identified outside the resected area, resulting in a very low PPV of 26.8%. The FPR for the NSF group was 7.5%, almost 13 times

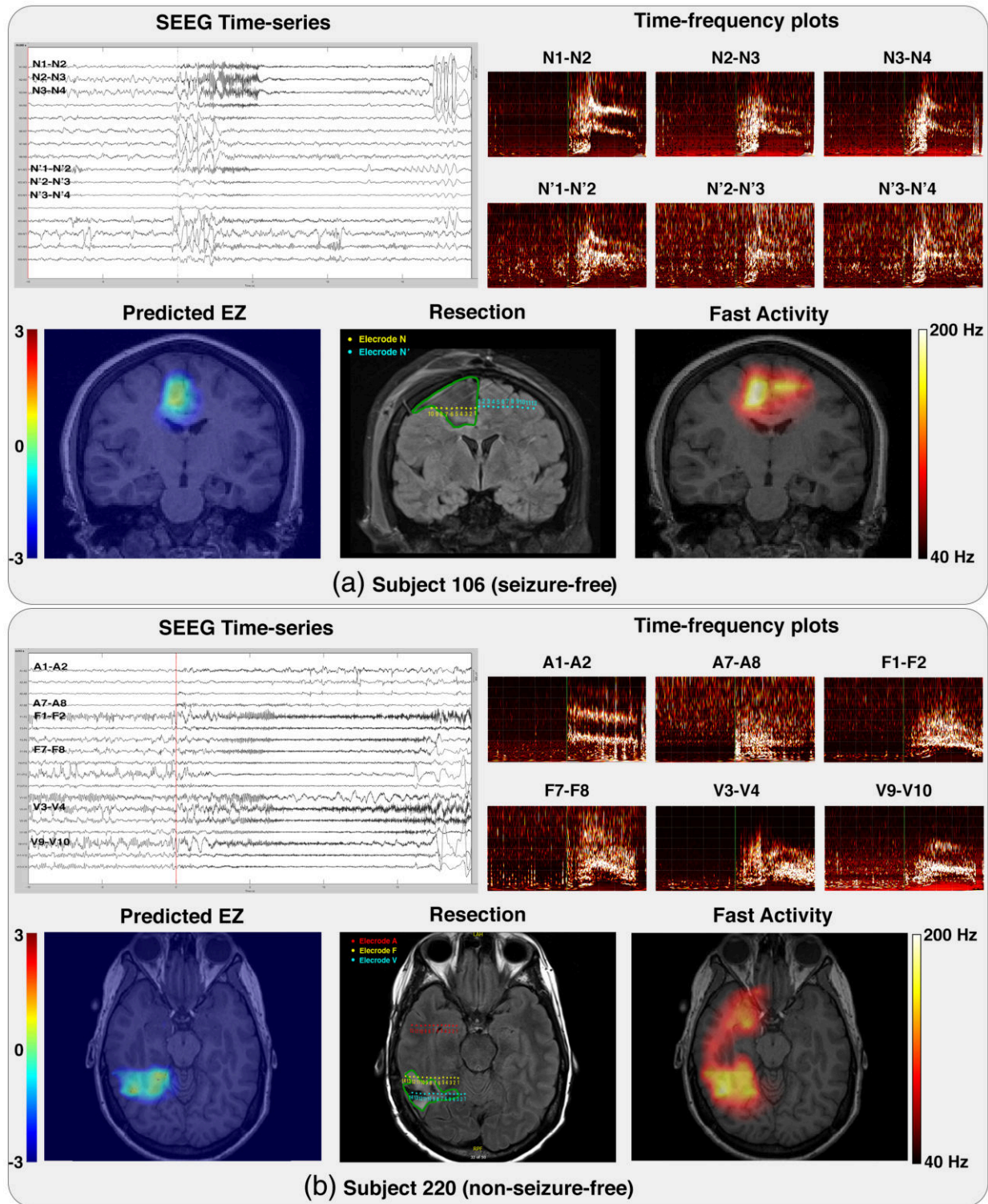


FIGURE 4 Two exemplar cases illustrating the epileptogenic zone fingerprint prediction (bottom-left) interpolated onto individual patients MRI in comparison with fast activity (bottom-right) and postoperative MRI (bottom-middle) with corresponding time series (top-left) and time-frequency plot (top-right) for electrodes of interest. (a) Subject 106 from the seizure-free group; (b) Subject 220 from the nonseizure-free group. Locations of the electrode contacts are illustrated in postoperative MRI where each color represents a distinct electrode. The boundary of the resection was drawn manually in green for illustrative purpose [Color figure can be viewed at wileyonlinelibrary.com]

bigger than that for the SF group (0.6%). Prediction results for each individual patient are shown in Table S2. Results without considering seizure clusters separately are shown in Table S3, where fewer EZ contacts were identified inside the resection, although similar PPV and FPR were obtained.

The true EZ is a priori unknown so we label true/false positive/negative (TP/FP/TN/FN) contacts with respect to the resected area. Since the resection tends to remove tissue beyond the boundaries of the EZ, we expect a large number of contacts to be classified as “false negatives” (FN) in both groups of patients in resected areas that are not in the true (but unknown) EZ.

Overall, we observed a large difference in EZ prediction results with respect to the resected regions between the SF group and the NSF group, although the same method was applied to both groups. Contacts identified by our EZ fingerprint were mostly localized within

the resection in the SF group, but a large fraction were outside the resection in the NSF group.

In this study we recruited patients with broader selection criteria relative to our earlier work (Grinenko et al., 2018). These new results show that the fingerprint pattern can also be identified in seizures initiated with frequencies as low as beta or even alpha band (See statistics in Figure 3).

Table 2b shows the prediction results when only FA features were used. A large number of contacts were predicted to be “EZ” but with a low PPV of 39.2%. For the SF group, 181 “EZ” contacts were localized inside the resection and 281 were outside the resection, suggesting that using only FA leads to an overestimation of the EZ.

Fingerprint-based EZ prediction results interpolated onto the patient's preoperative MRI are shown in Figure 4 for Subject 106 from the SF group, illustrating a complete resection of the predicted EZ, and Subject 220 from the NSF group, illustrating an incomplete resection of the predicted EZ. Similar results for all other subjects are shown in Figure S3. Additionally, Table 3 shows the relationships between the predicted EZ and resected areas (the predicted EZ was either fully resected or partially resected or not resected) and the surgical outcomes. Compared to the SF patients where the predicted EZ was almost always inside the resected area, hence they became SF after surgery, we observe that, for most of the NSF patients, the predicted EZ was either partially resected or not resected, which may explain the reason for the surgical failure in those cases.

In contrast to the EZ fingerprint, the FA was often more widely propagated and extended far beyond the EZ, although the EZ fingerprint and FA maps are partially colocalized (most often the EZ

TABLE 3 Comparison of the resection/laser ablation and surgical outcomes

Subject ID	Concordance of resection and predicted EZ ^a	Outcome (Engel)
101	(no EZ predicted)	1A
102 ^b	Complete	1A
103	(no EZ predicted)	1A
106	Complete	1A
108	Complete	1A
111	Complete	1A
112	Complete	1A
113	Partial	1A
116	Complete	1A
118	Complete	1A
140	(no EZ predicted)	1A
215	Predicted EZ not resected	2A
219	Partial	2A
220	Partial	4
221	(no EZ predicted)	3
222	Partial	2
223	Complete	3
226	Partial	2B
228	Predicted EZ not resected	4
231	Predicted EZ not resected	4
232	(no EZ predicted)	4
233	Complete	2
237	(no EZ predicted)	4
238	Partial	3

^aThe relationship between the resection and the predicted EZ was determined by visualization and manual inspection of the interpolated EZ prediction scores in the patient's MRI space.

^bThe false positive contact (only one) predicted in this patient (see Table S2) has a very low score relative to the true positive contacts, hence does not affect the overall estimate of the EZ. (See Figure S3 for details).

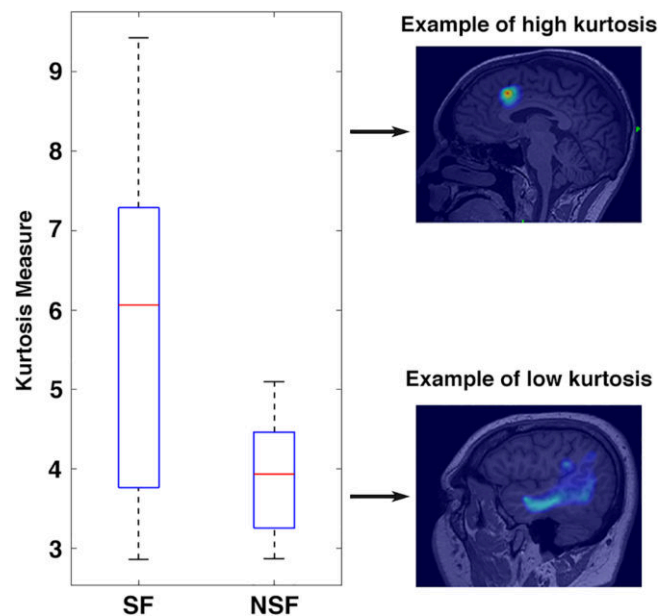


FIGURE 5 Boxplot of the kurtosis of the interpolated prediction scores for the seizure-free group on the left and the nonseizure-free group on the right. Example of the appearance of the epileptogenic zone fingerprint prediction that correspond to low and high kurtosis are shown on the right [Color figure can be viewed at wileyonlinelibrary.com]

fingerprint is a subset of the FA-identified EZ). For example, in Figure 4a, the fingerprint-based EZ area was unilateral and localized within the resected region while the FA-based EZ was in bilateral homotopic areas. This phenomenon can also be verified from the SEEG time series as well as the TF plots, with FA exhibited recorded from both electrodes N and N', although the appearance of fast activities differs across contacts. Since this patient (Figure 4a) was SF after surgery, the EZ was situated only in the right hemisphere. Hence, as noted above, it is very difficult to delineate EZ purely based on FA alone.

Overall, anatomical visualization of the predicted EZ showed a substantial difference in appearance between the SF group and the NSF group. In the SF group, the identified EZ usually presents as a restricted region within the resected area. On the other hand, in the NSF group the predicted EZ is usually more diffuse. Statistically, Figure 5 shows boxplots of the kurtosis across all subjects in the SF group on the left and the NSF group on the right. The kurtosis for the SF group is significantly higher than that for the NSF group with a one-sided p value of 3.8×10^{-3} for a student t test with 22 degree of freedom, indicating that the predicted EZ is more focal.

4 | DISCUSSION

4.1 | Validation of an EZ biomarker

Even though the concept of the "EZ" has been used for more than 50 years (Bancaud et al., 1965), its precise definition remains controversial, and a reliable biomarker is still missing. Several algorithms have been proposed to assess the extent of the EZ and compare it with either the EZ area identified by an expert clinician or the resected region (Andrzejak et al., 2014; Bartolomei et al., 2008; David et al., 2011; Gnatkovsky et al., 2011, 2014; Varatharajah et al., 2018). Some of these studies showed high concordance between the two.

However, the lack of ground truth and a precise definition of the EZ poses a significant challenge for us to validate the localization performance of a particular biomarker. First, there can be a large variation in ictal patterns across different subjects. Some waveform or time interval alterations may occur even across different seizures within subjects (see Figure 2a). Those latter alterations may not affect visual analysis based on the SEEG time series because an expert clinician will treat them as the same type with subtle differences in waveform. But they can significantly affect prediction results using machine-based algorithms and lead to underestimation of the EZ. Indeed, (Andrzejak et al., 2014) compared the performance of four earlier proposed approaches for automatic identification of the EZ (Andrzejak et al., 2014; Bartolomei et al., 2008; David et al., 2011; Gnatkovsky et al., 2011) and found that these methods produced highly discordant results depending on particular ictal patterns.

Moreover, the resected region is not an ideal ground truth for EZ either, because, as we discussed previously, the resected region is typically larger, sometimes much larger, than the actual EZ, resulting in a large number of FN predictions when using machine-based algorithms (Table 2), regardless of the seizure freedom of patients after surgery.

Instead of using the clinically defined EZ or the resected region as the ground truth, it would be more meaningful to compare the computer-assisted localization or prediction against long-term seizure outcomes after surgical treatment as it provides an objective criterion for evaluation of the accuracy of the EZ identification. Previous studies have shown that some features extracted from EEG and ECoG recordings, such as HFA (Jacobs et al., 2010) and phase-locked high gamma activity (PLHG) (Weiss et al., 2013), are correlated with Engel scores. Weiss et al. (2015) showed statistically significant difference of the Engel scores between the group of subjects where the area with early appearance of PLHG was resected and the group of subjects where that area was not resected. However, contradictory results have also been reported. For example, Blauwblomme et al. (2013) has shown that the epileptogenicity of insular cortex, measured with an earlier proposed algorithm (David et al., 2011), did not influence the outcome of temporal lobectomy, suggesting the difficulty of finding a reliable biomarker of the EZ.

Therefore, if a biomarker of EZ is a reliable one, the EZ should be identified or predicted exclusively within the resected region in patients that become long-term SF after surgery. On the other hand, the EZ should be either completely missed or only partially resected in NSF patients. The aim of this study was to validate the EZ fingerprint method on a completely independent set of patients that have been drawn with broader selection criteria including both SF and NSF subjects. To get a more realistic representation of the surgical plan, anatomical information was incorporated and the predicted EZ scores were mapped onto the patient's MRI space. Finally, we compared our fingerprint-based EZ prediction results with surgical outcome. The EZ prediction results (both the binary classification results and the interpolated imaging results) showed a substantial difference between the SF group and the NSF group. The predicted EZ was well localized inside the resected area in SF patients while it was not fully resected or completely missed in NSF patients. The contrast between the results for SF patients and that for NSF patients correlates with their surgical outcomes thus providing a posteriori explanation of the surgical success or failure in those cases.

4.2 | Fast activities yield EZ blurred images

FA has been increasingly used as a potential biomarker of the EZ since growing use of SEEG in presurgical evaluation. However, previous studies did not perform TF analysis so they could not differentiate between broad-band and narrow-band FAs. The former was frequently measured as the power of gamma activity that is much less discriminative than the latter in terms of EZ localization. For example, the epileptogenicity index (Bartolomei et al., 2008) emphasizes the analysis of FA and is calculated as the energy ratio between the fast frequencies (beta + gamma) and slow frequencies (theta + alpha). However, our TF analysis showed that beta and low gamma frequencies were often suppressed and the power in FA was highly variable. Also the epileptogenicity index mixes these two phenomena (high-frequency oscillations and low-frequency suppression) and does not account for the fact that frequency range and duration can vary

significantly both across subjects and between EZ and non-EZ areas. David et al. (2011) identified the EZ based on the maximal frequency of FA during early seizure spread. Gnatkovsky et al. (2011, 2014) measured the power of FA in a high gamma range and found that maximum power of high gamma activity correlated with a slow polarizing shift and less with EEG flattening. However, these studies either used FA solely or treated FA independently from other features.

To address the question of whether narrow-band FA, one of the three components of the fingerprint, can be an equally discriminative factor in localization of the EZ, we numerically classified EZ using features from FA only and mapped FA onto patient's MRI space using the same EZ fingerprint pipeline (Figure 1). Classification results showed a large number of false positive contacts outside the resected region (Table 2b). On the other hand, imaging results showed that the FA could extend/propagate to areas far beyond the EZ (Figure 4). Both results confirmed that the EZ was very difficult to localize and significantly over-estimated when (even narrow-band) FA only is used as a biomarker.

Moreover, as opposed to the previous studies where FA was usually defined as gamma activities or beyond, our analysis showed that the fingerprint patterns can be identified with frequency activities as low as beta or even alpha band (Figure 3), indicating the difficulty of EZ localization when using FA-based biomarkers with conventional but heuristic choice of frequency range.

4.3 | Automated EZ fingerprint classification pipeline

The proposed EZ fingerprint pipeline consists of four major parts: data preprocessing, fingerprint feature extraction, SVM-based classification, and MRI interpolation (Figure 1). To the best of our knowledge, this pipeline is the first complete end-to-end EZ prediction or estimation procedure that was validated based on long-term seizure outcome on a representative series of patients.

This machine-learning-based EZ fingerprint classification pipeline is crucial for successful application of the fingerprint method to delineate EZ from other areas because in many cases it is very difficult to distinguish EZ contacts from non-EZ contacts only by visual inspection of the TF plots. For example, the fingerprint pattern is clearly shown on the electrode N in Figure 4a, while the TF plots of electrode N' seem to have a blurred/vague version of the fingerprint. Based on visualization of this type of TF plots, it is not easy to deny the hypothesis that contacts on N' belong to the EZ area (while in fact N' is outside the EZ). The reason for this is because we are often looking for the existence of the fingerprint pattern during visual inspection but lack a proper evaluation of the typicality of the pattern (e.g., the narrow bands of FA are blurred, and the lower frequencies are not well suppressed on N' relative to N). In contrast, by taking all aspects of the fingerprint into account (i.e., all different types of features extracted from the TF plot), the SVM-based classification system is able to distinguish the pattern on N apart from that on N', hence yielding an accurate prediction of the EZ.

4.4 | Potential pitfalls in application of the EZ fingerprint method

Among all the steps in the EZ fingerprint pipeline, feature extraction is of particular importance due to the high complexity in the fingerprint patterns across subjects. As a result, the originally designed feature extraction steps might have been biased toward the set of 17 SF patients used in our previous study (Grinenko et al., 2018), in the sense that the parameters are tuned based on that set of patients and may not generalize well to other patients. For example, in Figure S2, the TF plot for Subject 103 shows a clear fingerprint pattern with a downchirping narrow-band FA. However, the slope of this banding is too steep to fall into the reasonable range ($\pm 45^\circ$ away from positive x-axis) that was designed to rule out false positive detections in the original dataset. Therefore, this FA was not successfully identified resulting in a missing prediction of the EZ.

Although the fingerprint pattern (the combination of preictal spike, narrow-band FA, and suppression) is very consistent across subjects, the individual features may vary substantially across subjects as well as across different seizures within subjects. For this reason, we found that prediction-score-based seizure clustering is an important step in the pipeline for good outcomes. In our original EZ fingerprint model an EZ contact predicted from a single cluster of seizures will yield no prediction if there is inconsistency in identified contacts from seizures in a different cluster. Results when considering different seizure clusters showed improved performance of EZ prediction over that without clustering. Here we use manual clustering. A systematic approach to clustering seizures and investigating the pathophysiological meaning behind different clusters may be of interest for future research.

Another possible pitfall of the fingerprint method may occur when the SEEG electrodes are not optimally placed. In that case it is almost impossible to delineate EZ from other areas based on the fingerprint method as the fingerprint pattern does not present or only partially presents if the electrode contact is not too distant from the core EZ area (e.g., Subject 101 and 140 in Figure S2). Nevertheless, in these cases, large resections may still include the EZ, hence patients may become SF after surgery even though no fingerprint has been identified. In fact, both the accuracy and the density of electrode implantations strongly affect and can be the bottleneck limiting the performance of the application of the fingerprint method to the EZ identification problem. Therefore, identifying a relatively accurate estimate of the EZ using presurgical noninvasive data, thus providing good guidance for electrode implantation, poses a challenging problem for the future.

Our observations in Figure 5 show that higher kurtosis is highly correlated with SF outcomes. In contrast, there may be multiple reasons for low kurtosis to occur in the interpolated EZ prediction images. For example, when the electrodes are not well placed so that the EZ is not sampled, the prediction scores will be low all over the brain. In other cases, the EZ may be large and diffuse but well sampled. There will then be a significant fraction of the brain that has high prediction values leading to a low kurtosis value. Conversely, when the kurtosis is high, then we have strong indication that the EZ is both

well sampled and resectable, leading to a higher chance of seizure freedom.

This study shows that the TF pattern described as a fingerprint of the EZ is a real marker of the cortical region, which should be resected or ablated to achieve seizure freedom for a given patient. FAs, as it spreads out of the EZ area, cannot be utilized separately from the other two elements of the fingerprint pattern for an accurate localization. Such inter-dependence reinforces the pathophysiological significance of the marker. As we discuss in more detail in Grinenko et al. (2018), this fits well with the model proposed by Avoli and de Curtis (Avoli & de Curtis, 2011; De Curtis & Avoli, 2016): progressive synchronized activation of pyramidal cells (low-frequency component of the preictal spikes) that excites disinhibited fast somatic inhibitory interneurons (FSIN) (fast-frequency component of the preictal spikes) leading to a sustained FSIN activation (ictal FAs) with pyramidal silencing as a consequence (suppression of low frequencies) (Avoli & de Curtis, 2011; Elahian, Yeasin, Mudigoudar, Wheless, & Babajani-Feremi, 2017; Fujiwara-Tsukamoto et al., 2010; Gnatkovsky, Librizzi, Trombin, & De Curtis, 2008; Truccolo et al., 2014; Weiss et al., 2016). At the end of the sustained FSIN discharge, rebound activation of pyramidal cells and interneurons occurs before the seizure stops. How the FAs resonate in a more extended network remains to be elucidated.

ACKNOWLEDGMENTS

The authors would like to thank the following treating physicians, whose patients were included in the study: Drs Juan Bulacio, Imad Najm, Dileep Nair, Andreas Alexopoulos, William Bingaman, Nancy Foldvary-Schaefer, Stephen Hantus, Lara Jehi, Elia Pestana Knight, Andrey Stojic, Ahsan Moosa Naduvil Valappil, and Ajay Gupta. We also would like to thank Ms Ping Liu and Drs Kenneth Taylor and Irene Wang for their technical support. Research reported in this publication was supported in part by the National Institutes of Health under award R01-NS089212, R01-EB009048 and R01-EB026299. The content is solely the responsibility of the authors and does not necessarily represent the official views of the National Institutes of Health.

CONFLICT OF INTEREST

The authors have no conflict of interests to declare.

DATA AVAILABILITY STATEMENT

The data that support the findings of this study are available on request from the corresponding author. The data are not publicly available due to privacy or ethical restrictions.

ORCID

Jian Li  <https://orcid.org/0000-0002-1691-8727>

Olesya Grinenko  <https://orcid.org/0000-0002-1950-8328>

John C. Mosher  <https://orcid.org/0000-0002-3221-229X>

Jorge Gonzalez-Martinez  <https://orcid.org/0000-0002-9936-7034>

Richard M. Leahy  <https://orcid.org/0000-0002-7278-5471>

Patrick Chauvel  <https://orcid.org/0000-0003-2161-6077>

REFERENCES

- Amidror, I. (2002). Scattered data interpolation methods for electronic imaging systems: A survey. *Journal of Electronic Imaging*, 11, 157. <https://doi.org/10.1117/1.1455013>
- Andrzejak, R. G., David, O., Gnatkovsky, V., Wendling, F., Bartolomei, F., Francione, S., ... de Curtis, M. (2014). Localization of epileptogenic zone on pre-surgical intracranial EEG recordings: Toward a validation of quantitative signal analysis approaches. *Brain Topography*, 28, 832–837. <https://doi.org/10.1007/s10548-014-0380-8>
- Avoli, M., & de Curtis, M. (2011). GABAergic synchronization in the limbic system and its role in the generation of epileptiform activity. *Progress in Neurobiology*, 95, 104–132. <https://doi.org/10.1016/j.pneurobio.2011.07.003>
- Bancaud, J., Talairach, J., Bonis, A., Schaub, C., Szikla, G., Morel, P., & Bordas-Ferer, M. (1965). *La stéréoelectroencéphalographie dans l'épilepsie. Informations neuro-physio-pathologiques apportées par l'investigation fonctionnelle stéréotaxique*. Paris, France: Masson. [https://doi.org/10.1016/0028-3932\(66\)90026-1](https://doi.org/10.1016/0028-3932(66)90026-1)
- Bartolomei, F., Chauvel, P., & Wendling, F. (2008). Epileptogenicity of brain structures in human temporal lobe epilepsy: A quantified study from intracerebral EEG. *Brain*, 131, 1818–1830. <https://doi.org/10.1093/brain/awn111>
- Blauwblomme, T., David, O., Minotti, L., Job, A. S., Chassagnon, S., Hoffman, D., ... Kahane, P. (2013). Prognostic value of insular lobe involvement in temporal lobe epilepsy: A stereoelectroencephalographic study. *Epilepsia*, 54, 1658–1667. <https://doi.org/10.1111/epi.12260>
- De Curtis, M., & Avoli, M. (2016). GABAergic networks jump-start focal seizures. *Epilepsia*, 57, 679–687. <https://doi.org/10.1111/epi.13370>
- David, O., Blauwblomme, T., Job, A. S., Chabards, S., Hoffmann, D., Minotti, L., & Kahane, P. (2011). Imaging the seizure onset zone with stereo-electroencephalography. *Brain*, 134, 2898–2911. <https://doi.org/10.1093/brain/awr238>
- Elahian, B., Yeasin, M., Mudigoudar, B., Wheless, J. W., & Babajani-Feremi, A. (2017). Identifying seizure onset zone from electrocorticographic recordings: A machine learning approach based on phase locking value. *Seizure*, 51, 35–42. <https://doi.org/10.1016/j.seizure.2017.07.010>
- Fujiwara-Tsukamoto, Y., Isomura, Y., Imanishi, M., Ninomiya, T., Tsukada, M., Yanagawa, Y., ... Takada, M. (2010). Prototypic seizure activity driven by mature hippocampal fast-spiking interneurons. *The Journal of Neuroscience*, 30, 13679–13689. <https://doi.org/10.1523/JNEUROSCI.1523-10.2010>
- Gnatkovsky, V., De Curtis, M., Pastori, C., Cardinale, F., Lo Russo, G., Mai, R., ... Francione, S. (2014). Biomarkers of epileptogenic zone defined by quantified stereo-EEG analysis. *Epilepsia*, 55, 296–305. <https://doi.org/10.1111/epi.12507>
- Gnatkovsky, V., Francione, S., Cardinale, F., Mai, R., Tassi, L., Lo Russo, G., & De Curtis, M. (2011). Identification of reproducible ictal patterns based on quantified frequency analysis of intracranial EEG signals. *Epilepsia*, 52, 477–488. <https://doi.org/10.1111/j.1528-1167.2010.02931.x>
- Gnatkovsky, V., Librizzi, L., Trombin, F., & De Curtis, M. (2008). Fast activity at seizure onset is mediated by inhibitory circuits in the entorhinal cortex in vitro. *Annals of Neurology*, 64, 674–686. <https://doi.org/10.1002/ana.21519>
- González Otárola, K. A., von Ellenrieder, N., Cuello-Oderiz, C., Dubeau, F., & Gotman, J. (2019). High frequency oscillation networks

- and surgical outcome in adult focal epilepsy. *Annals of Neurology*, 85(4), 485–494. <https://doi.org/10.1002/ana.25442>
- Grinenko, O., Li, J., Mosher, J. C., Wang, I. Z., Bulacio, J. C., Gonzalez-Martinez, J., ... Chauvel, P. (2018). A fingerprint of the epileptogenic zone in human epilepsies. *Brain*, 141, 117–131. <https://doi.org/10.1093/brain/awx306>
- Jacobs, J., Zijlmans, M., Zelmann, R., Chatillon, C. É., Hall, J., Olivier, A., ... Gotman, J. (2010). High-frequency electroencephalographic oscillations correlate with outcome of epilepsy surgery. *Annals of Neurology*, 67, 209–220.
- Lagarde, S., Buzori, S., Trebuchon, A., Carron, R., Scavarda, D., Milh, M., ... Bartolomei, F. (2019). The repertoire of seizure onset patterns in human focal epilepsies: Determinants and prognostic values. *Epilepsia*, 60(1), 85–95. <https://doi.org/10.1111/epi.14604>
- Shattuck, D. W., & Leahy, R. M. (2002). Brainsuite: An automated cortical surface identification tool. *Medical Image Analysis*, 6, 129–142. [https://doi.org/10.1016/S1361-8415\(02\)00054-3](https://doi.org/10.1016/S1361-8415(02)00054-3)
- Singh, S., Sandy, S., & Wiebe, S. (2015). Ictal onset on intracranial EEG: Do we know it when we see it? *State of the Evidence. Epilepsia*, 56, 1629–1638. <https://doi.org/10.1111/epi.13120>
- Tadel, F., Baillet, S., Mosher, J. C., Pantazis, D., & Leahy, R. M. (2011). Brainstorm: A user-friendly application for MEG/EEG analysis. *Computational Intelligence and Neuroscience*, 2011, 8. <https://doi.org/10.1155/2011/879716>
- Truccolo, W., Ahmed, O. J., Harrison, M. T., Eskandar, E. N., Cosgrove, G. R., Madsen, J. R., ... Cash, S. S. (2014). Neuronal ensemble synchrony during human focal seizures. *The Journal of Neuroscience*, 34, 9927–9944. <https://doi.org/10.1523/JNEUROSCI.4567-13.2014>
- Varatharajah, Y., Berry, B., Cimbalnik, J., Kremen, V., Van Gompel, J., Stead, M., ... Worrell, G. (2018). Integrating artificial intelligence with real-time intracranial EEG monitoring to automate interictal identification of seizure onset zones in focal epilepsy. *Journal of Neural Engineering*, 15, 046035. <https://doi.org/10.1088/1741-2552/aac960>
- Weiss, S. A., Banks, G. P., McKhann, G. M., Goodman, R. R., Emerson, R. G., Trevelyan, A. J., & Schevon, C. A. (2013). Ictal high frequency oscillations distinguish two types of seizure territories in humans. *Brain*, 136, 3796–3808.
- Weiss, S. A., Lemesiou, A., Connors, R., Banks, G. P., McKhann, G. M., Goodman, R. R., ... Schevon, C. A. (2015). Seizure localization using ictal phase-locked high gamma: A retrospective surgical outcome study. *Neurology*, 84, 2320–2328.
- Weiss, S. A., Alvarado-Rojas, C., Bragin, A., Behnke, E., Fields, T., Fried, I., ... Staba, R. (2016). Ictal onset patterns of local field potentials, high frequency oscillations, and unit activity in human mesial temporal lobe epilepsy. *Epilepsia*, 57, 111–121. <https://doi.org/10.1111/epi.13251>
- Westfall, P. H. (2014). Kurtosis as Peakedness. *The American Statistician*, 68, 191–195. <https://doi.org/10.1080/00031305.2014.917055>

SUPPORTING INFORMATION

Additional supporting information may be found online in the Supporting Information section at the end of this article.

How to cite this article: Li J, Grinenko O, Mosher JC, Gonzalez-Martinez J, Leahy RM, Chauvel P. Learning to define an electrical biomarker of the epileptogenic zone. *Hum Brain Mapp*. 2019;1–13. <https://doi.org/10.1002/hbm.24813>